scientific reports

Check for updates

OPEN

H_2-CO_2 polymer electrolyte fuel cell that generates power while evolving CH_4 at the $Pt_{0.8}Ru_{0.2}$/C cathode

Shofu Matsuda, Yuuki Niitsuma, Yuta Yoshida & Minoru Umeda✉

Generating electric power using CO_2 as a reactant is challenging because the electroreduction of CO_2 usually requires a large overpotential. Herein, we report the design and development of a polymer electrolyte fuel cell driven by feeding H_2 and CO_2 to the anode (Pt/C) and cathode ($Pt_{0.8}Ru_{0.2}$/C), respectively, based on their theoretical electrode potentials. Pt–Ru/C is a promising electrocatalysts for CO_2 reduction at a low overpotential; consequently, CH_4 is continuously produced through CO_2 reduction with an enhanced faradaic efficiency (18.2%) and without an overpotential (at 0.20 V vs. RHE) was achieved when dilute CO_2 is fed at a cell temperature of 40 °C. Significantly, the cell generated electric power (0.14 mW cm^{-2}) while simultaneously yielding CH_4 at 86.3 μmol g^{-1} h^{-1}. These results show that a H_2-CO_2 fuel cell is a promising technology for promoting the carbon capture and utilization (CCU) strategy.

Recently, carbon capture and utilization (CCU) methods have received significant levels of attention as technologies for effectively removing and utilizing atmospheric CO_2[1,2]. These technologies are attractive approaches as they treat CO_2 as an unused resource and convert it into value-added chemicals and fuels. Among them, electroreduction is a promising technique, and C_1, C_2, and C_{2+} products have reportedly been obtained using various electrocatalysts through different CO_2 reduction mechanisms[3–13]. In particular, CO production at Au and Ag, and hydrocarbon production at Cu, have been successfully elucidated to follow multistep proton-coupled electron-transfer pathways[14,15]. These reactions exhibit relatively high faradaic efficiencies; however, they require large overpotentials, which is disadvantageous. Consequently, their energy-conversion efficiencies are low, despite their high faradaic efficiencies.

Developing methods that ensure that the CO_2-electroreduction reaction occurs with a small overpotential and a high energy-conversion efficiency is important. In this regard, platinum group metals have the potential to realize overpotential-free CO_2 reductions. There are many reports in which CO is adsorbed on a metal (CO_{ads}) at a positive potential rather than its theoretical potential[16,17]. However, the further reduction of CO_{ads} is difficult because CO is strongly adsorbed to the metal through a donation–back-donation mechanism (Blyholder mechanism)[18]. To the best of our knowledge, the main product is H_2 when a Pt electrocatalyst is used, even when it is negatively polarized[19–21]. We previously obtained the C1 compound by reducing CO_2 near the theoretical potential in a proton-exchange-type membrane electrode assembly (MEA) with a carbon-supported platinum (Pt/C) electrocatalyst[22]. The use of a proton-exchange membrane and an ionomer was suggested to facilitate CO_2 reduction; however, the C1 yield was quite low. We recently demonstrated that CH_4 can be produced by the reduction of CO_2 in the absence of an overpotential and with a faradaic efficiency of 6.8% using the MEA[23]. This CH_4-generation reaction proceeds by a Langmuir–Hinshelwood (L–H) mechanism associated with CO_{ads} and H adsorbed on the metal (H_{ads}):

$$CO_{ads} + 6\,H_{ads} \rightarrow CH_4 + H_2O + 7^*, \quad (1)$$

where * represents an active site on the metal catalyst. It follows that placing CO_{ads} and H_{ads} in the appropriate ratio on the metal surface is important for CH_4 production, and this is realized by controlling the CO_2-feed concentration as well as the electrode potential in the case of a Pt catalyst[24]. Based on these techniques, we reported CO_2 reduction at a Pt catalyst to generate CH_4 with a faradaic efficiency of 12.3% at 0.16 V vs. RHE using 4 vol% CO_2 diluted with Ar (Ref.[25]).

Department of Materials Science and Technology, Graduate School of Engineering, Nagaoka University of Technology, 1603-1 Kamitomioka, Nagaoka, Niigata 940-2188, Japan. ✉email: mumeda@vos.nagaokaut.ac.jp

Here, the most noteworthy point is that the CH_4-synthesis potential is almost the same as the theoretical potential, which is more positive than that for the hydrogen oxidation reaction (HOR). Therefore, power can be generated by an H_2-CO_2 fuel cell[26] by combining the HOR and the CO_2 reduction reaction (to generate CH_4) as the anodic and cathodic reactions, respectively[25]. The H_2-CO_2 fuel cell is a promising CCU technology that utilizes CO_2 as a resource to generate electricity while producing a valuable compound (CH_4). However, the CH_4 yield as well as the amount of power generated need to be increased to further develop this technology, and the efficient use of CO_{ads}, which requires weakening the CO-metal bond, would represent a potential breakthrough toward this goal.

Pt-Ru alloy catalysts are known to impact the ligand effect, in which Ru affects the electronic state of CO_{ads} and weakens the CO-metal bond[27–30]. In our previous study, we investigated the reduction of CO_2 using MEAs incorporated with Pt-Ru electrocatalysts and revealed that the CH_4-generation efficiencies at the theoretical potential follow the order: Pt/C < $Pt_{0.5}Ru_{0.5}$/C < $Pt_{0.8}Ru_{0.2}$/C when 100 vol% CO_2 was supplied[31]. For this reason, we expected that CH_4 would be more-efficiently produced by the reduction of CO_2 without an overpotential by combining both techniques, namely diluting the CO_2 concentration and using a MEA with the $Pt_{0.8}Ru_{0.2}$/C electrocatalyst. In this work, we designed a polymer electrolyte fuel cell that incorporated a MEA with a $Pt_{0.8}Ru_{0.2}$/C cathode and a Pt/C anode. This paper reports the reduction of CO_2 for the simultaneous production of CH_4 and power by supplying CO_2 and H_2 to the cathode and anode, respectively.

Results

Effect of CO_2 concentration on CH_4 yield. We first performed cyclic voltammetry (CV) to assess the cathodic reaction of the prepared cell (Fig. 1a) under various CO_2 concentrations in Ar at a cell temperature of 40 °C. As shown in Fig. 1b, the oxidation current decreases with increasing CO_2 concentration in the 0.08–0.43 V (vs. RHE) potential range, whereas it increases between 0.43 and 0.70 V (vs. RHE). Considering that the former and the latter are the oxidation currents that originate from H desorption and CO desorption, respectively[32], this result reveals that the amounts of CO_{ads} and H_{ads} increase and decrease, respectively, with increasing CO_2 concentration. The faradaic charges for H_{ads} (Q_H) and CO_{ads} (Q_{CO}) calculated from Fig. 1b are shown in Fig. 1c. In detail, Q_H and Q_{CO} were calculated as the integrated faradaic oxidation currents at 0.08–0.43 V (vs. RHE) and 0.43–0.70 V (vs. RHE), respectively, as depicted as the green filled area (for Q_H) and the red filled area (for Q_{CO}) in the inset in Fig. 1c. Based on Fig. 1c, a trade-off relationship between the Q_{CO} and Q_H are clearly observed. Therefore, the amounts of CO_{ads} and H_{ads} on the $Pt_{0.8}Ru_{0.2}$/C catalyst surface can be controlled by changing the concentration of CO_2 supplied to the cathode. The onset potential for CO_{ads} desorption was determined, as shown by the black arrow in Fig. 1b, which provided a value of 0.43 V (vs. RHE) for $Pt_{0.8}Ru_{0.2}$/C, which is more negative than that for Pt/C (0.45 V vs. RHE[25]), suggesting that the $Pt_{0.8}Ru_{0.2}$/C electrocatalyst exhibits a lower CO-adsorption energy.

CH_4 generation from CO_2 reduction at the $Pt_{0.8}Ru_{0.2}$/C electrocatalyst was next investigated. Figure 2a,b show cyclic voltammograms with in-line MS signals (m/z 2 and 15) at CO_2 concentrations of 7 vol% and 100 vol%, respectively. The signal at m/z 15 was simultaneously detected with a reduction current at 7 vol% CO_2 when the potential was below ~ 0.25 V (vs. RHE), whereas the m/z 15 signal only was weakly detected at 100 vol% CO_2. The pattern in the mass spectrum of the cathodic output gas from the cell at 0.10 V (vs. RHE) in the 7 vol% CO_2 atmosphere (Supplementary Fig. S1) is concordant with that of the CH_4 standard gas; hence, the detected signal at m/z 15, which corresponds to CH_3^+ (not affected by H_2O and CO_2), is entirely derived from CH_4 produced through the reduction of CO_2. It should be noted that the signal at m/z 2 as hydrogen generation started to be detected at ~ 0.08 V (vs. RHE) at all CO_2 concentrations. Figure 2c shows the dependence of the faradaic efficiency determined during CH_4 generation on the CO_2 concentration acquired during negative-potential-sweep CV between 0.20 and 0.10 V (vs. RHE). The faradaic efficiency was determined as a percentage of the methanogenic faradaic charge relative to the total faradaic charge. As a result, the highest faradaic efficiency of ~ 4.5% was calculated at 7 vol% CO_2, which exceeds the efficiency for Pt/C (3.0% in a 5 vol% CO_2 atmosphere[24]). On the other hand, the faradaic efficiency was only 0.61% in 100 vol% CO_2, which corresponds to our previously reported efficiency[31]. Overall, we determined 7 vol% to be the preferred CO_2 concentration for generating CH_4 at the $Pt_{0.8}Ru_{0.2}$/C electrocatalyst.

CH_4-generation dependence on the CO_2 electroreduction potential. We next explored the optimum potential for CH_4 production at the $Pt_{0.8}Ru_{0.2}$/C electrocatalyst with the supplied CO_2 concentration fixed at 7 vol% under a potentio-static condition. The cathode potential was stepped 14 times in the negative direction in the 0.40–0.05 V (vs. RHE) range every 2 min. As shown in Fig. 3a, which was produced by analyzing Supplementary Fig. S2, the signal at m/z 15 for CH_4 began to be detected at 0.30 V (vs. RHE), was most intense at around 0.20 V (vs. RHE), and began to decrease in intensity below this value. The cathode potential at which the maximum m/z 15 signal was observed was different under the potentio-dynamic (Fig. 2a) and potentio-static (Fig. 3a) conditions, probably be due to the slow reaction rate of $CO_2 \rightarrow CH_4$. Meanwhile, the signal at m/z 2 for H_2 was observed only at 0.08 V and 0.05 V (vs. RHE), where CH_4 generation was suppressed. These results reveal that CH_4 production occurs at a more positive potential than H_2 evolution, with a maximum CH_4 yield observed at 0.20 V (vs. RHE). The in-line MS signals (m/z 2 and 15) recorded during cyclic voltammetry at 0 vol% CO_2 (100 vol% Ar) shown in Supplementary Fig. S3 reveal that the m/z 15 signal was hardly detected at all cathode potentials. Based on the standard $CO_2|CH_4$ electrode potential (0.169 V vs. SHE[33]), we successfully generated CH_4 from CO_2 in the absence of an overpotential in this study. Therefore, from the viewpoints of CH_4 yield and product selectivity, 0.20 V vs. RHE was determined to be the preferred potential.

We subsequently directly stepped the potential from 0.40 to 0.20 V (vs. RHE). As shown in Fig. 3b, the intensity of the m/z 15 signal was observed to be almost constant when the potential was held at 0.20 V (vs. RHE).

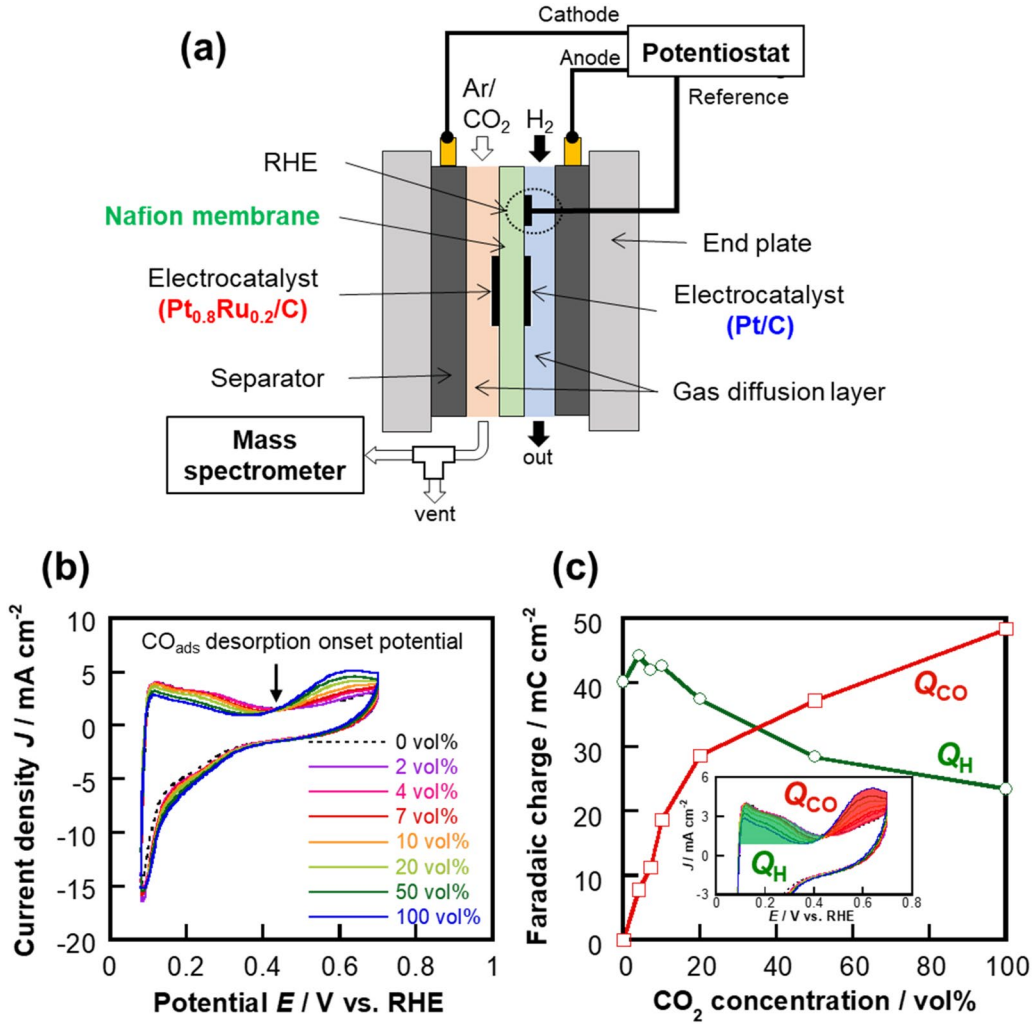

Figure 1. Schematic diagram and performance data. (**a**) Schematic diagram of the experimental setup used in this study. (**b**) Cathodic cyclic voltammograms at various concentrations of CO_2 in Ar. (**c**) CO_2-concentration-dependences of the faradaic charges of the oxidation-current peaks between 0.08 and 0.43 V (Q_H) and between 0.43 and 0.70 V (Q_{CO}) (vs. RHE) in the voltammograms shown in (**b**). The method used to calculate Q_H and Q_{CO} is shown in the inset in panel (**c**).

The faradaic efficiency of CH_4 generation from CO_2 reduction ($CO_2 + 8H^+ + 8e^- \rightarrow CH_4 + 2H_2O$) between 240 and 299 s in Fig. 3b was calculated by the following formula:

$$\text{Faradaic efficiency (\%)} = \frac{nmF}{It} \times 100, \tag{2}$$

where n is the number of reaction electrons, m is the molar number of CH_4, F is the Faraday constant, I is the mean current, and t is the time. Significantly, the faradaic efficiency was 18.2%, which exceeds the previously reported Pt/C efficiency (12.3%[25]). Supplementary Fig. S4 shows gas chromatograms of the cathodic output gas from the cell in which the cathode potential was held at 0.20 V (vs. RHE). Based on the results obtained using flame-ionization and thermal-conductivity detectors, only CH_4 was produced during CO_2 reduction at $Pt_{0.8}Ru_{0.2}$/C, and the faradaic efficiency was calculated to be 17.6%, as detailed in Supplementary Information S4. Overall, continuous CH_4 generation with enhanced efficiency and zero overpotential was achieved at a CO_2 concentration of 7 vol% and a holding potential of 0.20 V (vs. RHE).

Power generation as an H_2-CO_2 fuel cell. Figure 4 shows power generation characteristics as well as CH_4-production rates determined from the data in Fig. 3a. The current densities shown in Fig. 4 are mean current densities (shown in Supplementary Fig. S2) for 60 s just before the next potential step. Figure 4 reveals that the power density (as an H_2-CO_2 fuel cell) and the CH_4 yield rate exhibit similar trends, with maximum values of ~ 0.14 mW cm^{-2} and 86.3 μmol g^{-1} h^{-1}, respectively, at a cell voltage of 0.20 V. Compared to a report on the

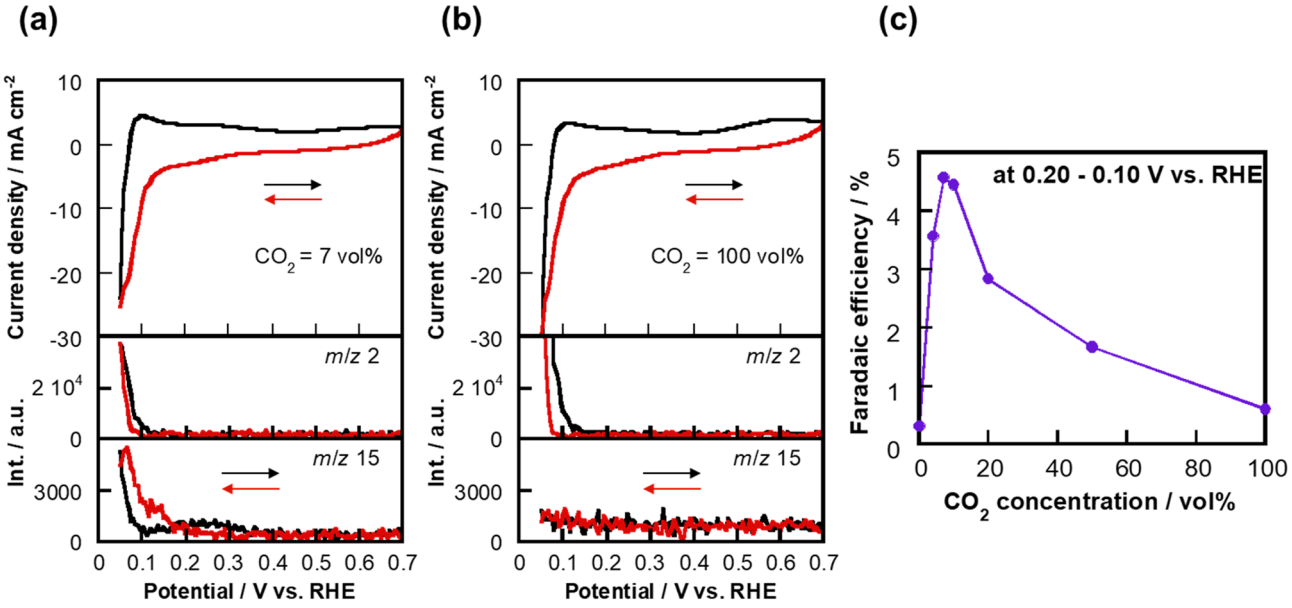

Figure 2. Cyclic voltammetry coupled with mass spectrometry. In-line *m*/*z* 2 (for H_2) and 15 (for CH_4) MS signals during CV at CO_2 concentrations of: (**a**) 7 vol% and (**b**) 100 vol%. (**c**) Faradaic efficiency for the generation of CH_4 as a function of CO_2 concentration calculated by integrating the *m*/*z* 15-signals in the 0.20–0.10 V (vs. RHE) potential range during negative-scan CV.

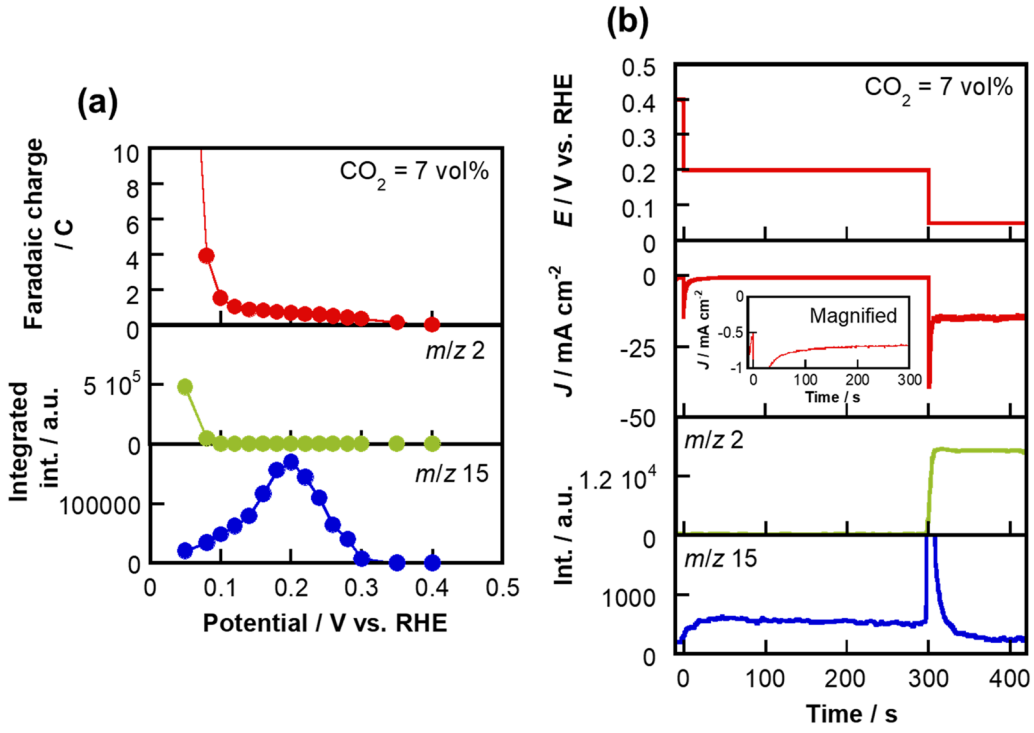

Figure 3. Stationary-potential CO_2 reduction. (**a**) Potential dependence of faradaic charge, and integrated *m*/*z* 2 and 15 MS signals when held at each potential for 2 min at a CO_2 concentration of 7 vol%. (**b**) Potential program applied to the cathode (upper), current response (middle), and in-line *m*/*z* 2 and 15 MS signals (lower) at 7 vol% CO_2.

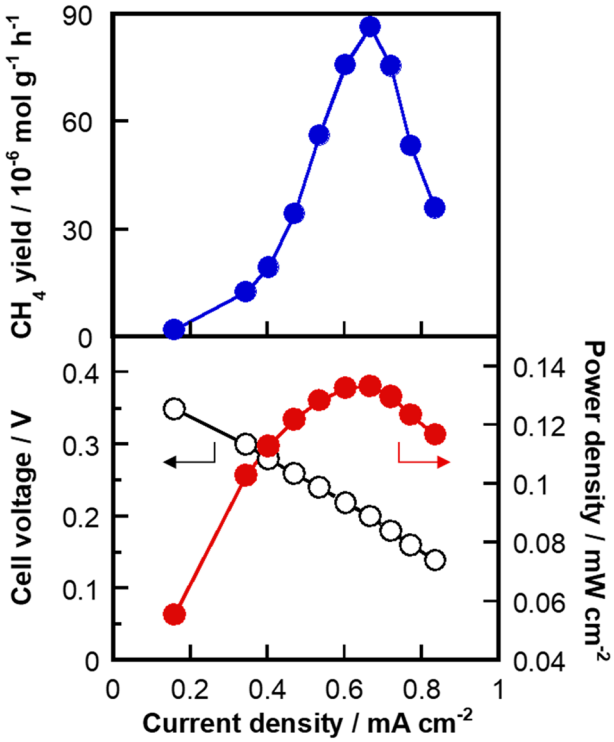

Figure 4. Cell performance. CH_4 yield, cell voltage, and power density as functions of current density at a CO_2 concentration of 7 vol%.

	$Pt_{0.8}Ru_{0.2}/C$	Pt/C
Cell voltage/V	0.20	0.16
Power density/mW cm^{-2}	0.14	0.015
CH_4 yield rate/μmol g^{-1} h^{-1}	86.3	26.4
Turnover frequency/nmol $(ECSA)^{-1}$ s^{-1}	0.73	0.15
Faradaic efficiency/%	18.2	12.3

Table 1. Comparing $Pt_{0.8}Ru_{0.2}/C$ and Pt/C cathode electrocatalyst data for the H_2-CO_2 fuel cell. Pt/C data are taken from our previous report[25].

formation of CH_3OH (but not CH_4) through CO_2 reduction at Pt–Ru/C using a MEA[34], the rate of CH_4 production in this study is higher.

Finally, we compared the results obtained for $Pt_{0.8}Ru_{0.2}/C$ with those for Pt/C. As listed in Table 1, the power density, CH_4 yield rate, turnover frequency, and faradaic efficiency were ~ 10-, ~ 3.5-, ~ 5-, and ~ 1.5-times higher, respectively, when the $Pt_{0.8}Ru_{0.2}/C$ electrocatalyst was used instead of the Pt/C electrocatalyst. Therefore, we demonstrated a H_2-CO_2 fuel cell that generates electric power while efficiently reducing CO_2 to CH_4.

Discussion

In the present study, we designed and demonstrated an H_2-CO_2 polymer-electrolyte fuel cell that generates CH_4 from CO_2 with enhanced efficiency, which was achieved by the strategic use of a $Pt_{0.8}Ru_{0.2}/C$ cathodic catalyst. As mentioned in the introduction, the generation of CH_4 through the reduction of CO_2 follows the L–H mechanism involving CO_{ads} and H_{ads} (Ref.[23]). According to Eq. (1), this reaction theoretically proceeds at a CO_{ads}-to-H_{ads} molar ratio of 1:6; however, this reaction proceeded when the ratio was 1:11 or higher for a Pt/C electrocatalyst[24], with the best ratio reported to be 1:18 (Ref.[24]). On the other hand, this ratio at the $Pt_{0.8}Ru_{0.2}/C$ electrocatalyst was determined to be 1:8 at a CO_2 concentration of 7 vol% according to the following equation:

$$CO_{ads} : H_{ads} = \left(\frac{Q_{CO}}{2}\right) : Q_H. \quad (3)$$

Hence, CO_{ads} can be used to efficiently generate CH_4 at $Pt_{0.8}Ru_{0.2}$/C because the ratio is close to the theoretical value of 1:6, which leads to a higher faradaic CH_4-production efficiency, and was achieved by the lower CO-adsorption energy associated with the $Pt_{0.8}Ru_{0.2}$/C electrocatalyst.

The sustained generation of CH_4 at 0.20 V (vs. RHE) (Fig. 3b) is also related to the CO_{ads}-to-H_{ads} ratio. Based on Supplementary Fig. S5, this ratio was determined to be 1:7 after holding at a potential of 0.20 V (vs. RHE) for 5 min at 7 vol% CO_2. Therefore, CH_4 is continuously generated at $Pt_{0.8}Ru_{0.2}$/C because the CO_{ads}-to-H_{ads} ratio was slightly different when the potential was held at 0.20 V (vs. RHE). It should be noted that the CH_4-production reaction proceeds at a more-positive potential than its theoretical potential. Although the reason is unclear at present, there is one possible explanation for this observation. In our system, the $CO_2|CH_4$ equilibrium potential is influenced by the proton activity of the Nafion membrane electrolyte. As shown in Supplementary Fig. S3, the H_2-evolution onset potential is ~ 0.08 V (vs. RHE); this value does not correspond to the theoretical potential (0.00 V vs. SHE[33]). In addition, the proton activity of the Nafion membrane has been reported to be different to that observed under SHE conditions[35–37]. Importantly, the CH_4-generation reaction is likely to occur through a sequential $CO_2 \rightarrow CO_{ads} \rightarrow CH_4$ reduction process, rather than through a one-step process ($CO_2 \rightarrow CH_4$). Supplementary Fig. S6 shows that the onset potential for the formation of CO_{ads} from CO_2 through reduction at $Pt_{0.8}Ru_{0.2}$/C in 7 vol% CO_2 is 0.375 V (vs. RHE). Hence, an electrode potential that progresses the $CO_{ads} \rightarrow CH_4$ process can drive the overall reaction.

H_2-CO_2 fuel cells function when platinum group metals are employed as cathodic catalysts. In other words, a H_2-CO_2 fuel cell does not function using "active" electrocatalysts composed of only Cu, Au, and Ag, as well as their alloys, because CO_2 reduction proceeds at a more negative potential than that for HOR (the overpotential is large)[38]. It should be noted that the highest faradaic CH_4-yield efficiency was only 18.2% in this study, which is insufficient for practical applications. The reason for this low efficiency has not yet been clarified; one possible process that contributes to the rest efficiency involves the formation of CO_{ads} and H_{ads}, which are not associated with CH_4 generation. Hence, further increasing the efficiency through catalyst design, including optimizing the Ru ratio in the Pt-Ru catalyst, will be important. One significant advantage of this technology is that the CO_2-conversion reaction that produces CH_4 occurs at a lower temperature (40 °C) than that used in chemical methanation technology[39] and CO_2-utilization technologies that rely on solid oxide electrolytes[40] and molten solts[41], which require temperature of several hundreds of degrees.

In conclusion, this work provides a novel approach to H_2-CO_2 fuel cells as a CO_2-utilization technology. CH_4 is produced continuously by the reduction of CO_2 in the absence of an overpotential (at 0.20 V vs. RHE) in a cell that uses a MEA with a $Pt_{0.8}Ru_{0.2}$/C cathode at a CO_2 concentration of 7 vol% and a cell temperature of 40 °C, and electrical energy is generated by combining the CO_2-reduction and H_2-oxidation (at a Pt/C anode) reactions. These results facilitate the carbon utilization strategy, although further investigations are necessary before it can be considered for practical applications.

Methods

Materials. $Pt_{0.8}Ru_{0.2}$/C (42.5 wt%; TECRuE43) and Pt/C (46.2 wt%; TEC10E50E) electrocatalyst powders were obtained from Tanaka Kikinzoku Kogyo Co., Ltd. Nafion-117 membranes (0.18-mm thick) were purchased from DuPont and boiled successively in Milli-Q water, 0.5 M H_2O_2, 0.5 M H_2SO_4, and Milli-Q water (1 h each) prior to use. All chemicals (H_2O_2, H_2SO_4, acetone, 2-propanol, methanol, and 5 wt% Nafion solution) were obtained from the Fujifilm Wako Pure Chemical Corporation. Water-repellent carbon paper (TGP-H-060H) was purchased from Toray Industries, Inc, and polymer electrolyte cell components (gasket, separator with parallel flow paths, and stainless steel plate) were purchased from Miclab.

Cell fabrication. A polymer electrolyte fuel cell (PEFC) was fabricated by essentially following the same procedure reported previously[23–25], with the exception that $Pt_{0.8}Ru_{0.2}$/C was used as the cathode instead of Pt/C. Briefly, a 6×6 cm^2 Nafion 117 membrane and 3×3 cm^2 pieces of carbon paper pretreated with acetone were used as the proton-exchange membrane and gas diffusion layers, respectively. The electrocatalyst dispersion was prepared by mixing the $Pt_{0.8}Ru_{0.2}$/C catalyst with 5 wt% Nafion (1:1 v/v) and an aqueous solution containing 1:2:1 (w/w/w) 2-propanol, methanol, and Milli-Q water, followed by spraying onto one piece carbon paper to prepare the cathode. The anode was prepared by spraying a Pt/C electrocatalyst dispersion onto another piece of carbon paper. The amount of loaded metal and the apparent electrode surface area were 1.0 mg cm^{-2} and 9.0 cm^2, respectively, on both electrodes. The MEA was prepared by bringing these electrodes into contact with each side of the Nafion-117 membrane, followed by hot-pressing at 140 °C with a 4.5 kN load for 10 min. It should be noted that the Pt/C electrocatalyst dispersion was dropped onto the Nafion 117 membrane on the anode side to provide a reference reversible hydrogen electrode (RHE). Finally, the MEA, gasket, separator, and stainless steel plate were assembled to complete the PEFC used in this study, as shown in Fig. 1a.

Electrochemical CO_2 reduction and product analysis. A schematic diagram of the experimental setup used in this study is shown in Fig. 1a. Electrochemical experiments were conducted using a PEFC-operating apparatus (FCG-20S, ACE), a potentiostat/galvanostat (HA-310, Hokuto Denko), and a function generator (HB-104, Hokuto Denko). Fully humidified 100 vol% H_2 and CO_2 diluted with Ar (CO_2 concentration: 0, 4, 7, 10, 20, 50, and 100 vol%) gas were fed to the anode and cathode at 50 cm^3 min^{-1}, respectively, in all experiments. Fully humidified 100 vol% H_2 gas was supplied to the reference electrode at 10 cm^3 min^{-1}. The cell temperature was set to 40 °C because the cell humidification at least 40 °C is required to operate the MEA. The H_2, CO_2, and Ar gases were 99.999%, 99.995%, and 99.998% pure, respectively. Before electrochemical measurements, the cathodic potential sweep in the 0.05–0.70 V (vs. RHE) range at 50 mV s^{-1} was repeated until the current–potential curve of the cathode became stable. The initial cathode potential during introduction of CO_2-containing gas

was ~ 0.13 V (vs. RHE). The electrochemical surface area (ECSA) of the cathode electrocatalyst was obtained to be 0.294 m^2 according to the hydrogen adsorption method[30,42,43]. The cathodic potential was scanned in the 0.08–0.70 V (vs. RHE) range at 10 mV s^{-1} during CV. It should be noted that that a 0.05–0.70 V (vs. RHE) potential range was used for CV with in-line product analysis. In the potential-step experiment, the cathodic potential was stepped through 14 levels in the 0.40–0.05 V (vs. RHE) range in the negative direction every 2 min at a CO_2 concentration of 7 vol%. In addition, the cathodic potential was directly stepped from 0.40 to 0.20 V (vs. RHE) at 7 vol% CO_2 and held there for 5 min, after which it was stepped to 0.05 V (vs. RHE). In-line mass spectrometry (MS) was carried out during the electrochemical experiments by introducing the cathode exhaust gas directly to a mass spectrometer (JMS-Q1050GC, JEOL). The ionization voltage was 23 eV. Note that the lag time for in-line MS product detection was adjusted by the H_2 evolution response (7 s). A calibration curve, which was obtained using CH_4 gas (purity: 99.999%) diluted with Ar, was used to calculate the amount of CH_4 generated, for determining the faradaic efficiencies and CH_4-yield rates. All the current densities were calculated using the apparent electrode surface area (9.0 cm^2).

Received: 8 December 2020; Accepted: 5 April 2021
Published online: 16 April 2021

References

1. Hepburn, C. *et al.* The technological and economic prospects for CO_2 utilization and removal. *Nature* **575**, 87–97. https://doi.org/10.1038/s41586-019-1681-6 (2019).
2. Abanades, J. C., Rubin, E. S., Mazzotti, M. & Herzog, H. J. On the climate change mitigation potential of CO_2 conversion to fuels. *Energy Environ. Sci.* **10**, 2491–2499. https://doi.org/10.1039/C7EE02819A (2017).
3. Liu, M. *et al.* Enhanced electrocatalytic CO_2 reduction via field-induced reagent concentration. *Nature* **537**, 382–386. https://doi.org/10.1038/nature19060 (2016).
4. Hossain, M. H., Wen, J. & Chen., A. Unique copper and reduced graphene oxide nanocomposite toward the efficient electrochemical reduction of carbon dioxide. *Sci. Rep.* **7**, 3184. https://doi.org/10.1038/s41598-017-03601-3 (2017).
5. Liu, S. *et al.* Shape-dependent electrocatalytic reduction of CO_2 to CO on triangular silver nanoplates. *J. Am. Chem. Soc.* **139**, 2160–2163. https://doi.org/10.1021/jacs.6b12103 (2017).
6. Nguyen, D. L. T. *et al.* Selective CO_2 reduction on zinc electrocatalyst: The effect of zinc oxidation state induced by pretreatment environment. *ACS Sustainable Chem. Eng.* **5**, 11377–11386. https://doi.org/10.1021/acssuschemeng.7b02460 (2017).
7. Li, F., Chen, L., Knowles, P. G., MacFarlane, D. R. & Zhang, J. Hierarchical mesoporous SnO_2 nanosheets on carbon cloth: a robust and flexible electrocatalyst for CO_2 reduction with high efficiency and selectivity. *Angew. Chem. Int. Ed.* **56**, 505–509. https://doi.org/10.1002/anie.201608279 (2017).
8. Wu, Y., Jiang, Z., Lu, X., Liang, Y. & Wang, H. Domino electroreduction of CO_2 to methanol on a molecular catalyst. *Nature* **575**, 639–642. https://doi.org/10.1038/s41586-019-1760-8 (2019).
9. Choi, J. *et al.* Energy efficient electrochemical reduction of CO_2 to CO using a three-dimensional porphyrin/graphene hydrogel. *Energy Environ. Sci.* **12**, 747–755. https://doi.org/10.1039/C8EE03403F (2019).
10. Zhang, E. *et al.* Bismuth single atoms resulting from transformation of metal–organic frameworks and their use as electrocatalysts for CO_2 reduction. *J. Am. Chem. Soc.* **141**, 16569–16573. https://doi.org/10.1021/jacs.9b08259 (2019).
11. Todoroki, N. *et al.* Surface atomic arrangement dependence of electrochemical CO_2 reduction on gold: online electrochemical mass spectrometric study on low-index Au(*hkl*) Surfaces. *ACS Catal.* **9**, 1383–1388. https://doi.org/10.1021/acscatal.8b04852 (2019).
12. Kim, T. & Palmore, T. R. A scalable method for preparing Cu electrocatalysts that convert CO_2 into C_{2+} products. *Nat. Commun.* **11**, 3622. https://doi.org/10.1038/s41467-020-16998-9 (2020).
13. Arán-Ais, R. M. *et al.* Imaging electrochemically synthesized Cu_2O cubes and their morphological evolution under conditions relevant to CO_2 electroreduction. *Nat. Commun.* **11**, 3489. https://doi.org/10.1038/s41467-020-17220-6 (2020).
14. Kortlever, R., Shen, J., Schouten, K. J. P., Calle-Vallejo, F. & Koper, M. T. M. Catalysts and reaction pathways for the electrochemical reduction of carbon dioxide. *J. Phys. Chem. Lett.* **6**, 4073–4082. https://doi.org/10.1021/acs.jpclett.5b01559 (2015).
15. Peterson, A. A., Abild-Pedersen, F., Studt, F., Rossmeisl, J. & Nørskov, J. K. How copper catalyzes the electroreduction of carbon dioxide into hydrocarbon fuels. *Energy Environ. Sci.* **3**, 1311–1315. https://doi.org/10.1039/C0EE00071J (2010).
16. Giner, J. Electrochemical reduction of CO_2 on platinum electrodes in acid solutions. *Electrochim. Acta* **8**, 857–865. https://doi.org/10.1016/0013-4686(63)80054-7 (1963).
17. Hori, Y. Electrochemical CO_2 reduction on metal electrodes. *Mod. Aspects Electrochem.* **42**, 89–189. https://doi.org/10.1007/978-0-387-49489-0_3 (2008).
18. Koper, M. T. M. & van Santen, R. A. Electric field effects on CO and NO adsorption at the Pt(111) surface. *J. Electroanal. Chem.* **476**, 64–70. https://doi.org/10.1016/S0022-0728(99)00367-8 (1999).
19. Hori, Y., Wakebe, H., Tsukamoto, T. & Koga, O. Electrocatalytic process of CO selectivity in electrochemical reduction of CO_2 at metal electrodes in aqueous media. *Electrochim. Acta* **39**, 1833–1839. https://doi.org/10.1016/0013-4686(94)85172-7 (1994).
20. Kuhl, K. P. *et al.* Electrocatalytic conversion of carbon dioxide to methane and methanol on transition metal surfaces. *J. Am. Chem. Soc.* **136**, 14107–14113. https://doi.org/10.1021/ja505791r (2014).
21. Lee, J., Lim, J., Roh, C.-W., Whang, H. S. & Lee, H. Electrochemical CO_2 reduction using alkaline membrane electrode assembly on various metal electrodes. *J. CO_2 Util.* **31**, 244–250. https://doi.org/10.1016/j.jcou.2019.03.022 (2019).
22. Shironita, S., Karasuda, K., Sato, M. & Umeda, M. Feasibility investigation of methanol generation by CO_2 reduction using Pt/C-based membrane electrode assembly for a reversible fuel cell. *J. Power Sources* **228**, 68–74. https://doi.org/10.1016/j.jpowsour.2012.11.097 (2013).
23. Umeda, M., Niitsuma, Y., Horikawa, T., Matsuda, S. & Osawa, M. Electrochemical reduction of CO_2 to methane on platinum catalysts without overpotentials: strategies for improving conversion efficiency. *ACS Appl. Energy Mater.* **3**, 1119–1127. https://doi.org/10.1021/acsaem.9b02178 (2020).
24. Matsuda, S. *et al.* Minimization of Pt-electrocatalyst deactivation in CO_2 reduction using a polymer electrolyte cell. *React. Chem. Eng.* **5**, 1064–1070. https://doi.org/10.1039/d0re00083c (2020).
25. Umeda, M., Yoshida, Y. & Matsuda, S. Highly selective methane generation by carbon dioxide electroreduction on carbon-supported platinum catalyst in polymer electrolyte fuel cell. *Electrochim. Acta* **340**, 135945. https://doi.org/10.1016/j.electacta.2020.135945 (2020).
26. Umeda, M., Sato, M., Maruta, T. & Shironita, S. Is power generation possible by feeding carbon dioxide as reducing agent to polymer electrolyte fuel cell?. *J. Appl. Phys.* **114**, 174908. https://doi.org/10.1063/1.4829030 (2013).

27. Waszczuk, P. *et al.* Adsorption of CO poison on fuel cell nanoparticle electrodes from methanol solutions: A radioactive labeling study. *J. Electroanal. Chem.* **511**, 55–64. https://doi.org/10.1016/S0022-0728(01)00559-9 (2001).
28. Christoffersen, E., Liu, P., Ruban, A., Skriver, H. L. & Nørskov, J. K. Anode materials for low-temperature fuel cells: A density functional theory study. *J. Catal.* **199**, 123–131. https://doi.org/10.1006/jcat.2000.3136 (2001).
29. Wakisaka, M. *et al.* Electronic structures of Pt-Co and Pt-Ru alloys for CO tolerant anode catalysts in polymer electrolyte fuel cells studied by EC-XPS. *J. Phys. Chem. B* **110**, 23489–23496. https://doi.org/10.1021/jp0653510 (2006).
30. Furukawa, H., Matsuda, S., Tanaka, S., Shironita, S. & Umeda, M. CO_2 electroreduction characteristics of Pt-Ru/C powder and Pt-Ru sputtered electrodes under acidic condition. *Appl. Surf. Sci.* **434**, 681–686. https://doi.org/10.1016/j.apsusc.2017.10.219 (2018).
31. Niitsuma, Y., Sato, K., Matsuda, S., Shironita, S. & Umeda, M. CO_2 reduction performance of Pt-Ru/C electrocatalyst and its power generation in polymer electrolyte fuel cell. *J. Electrochem. Soc.* **166**, F208–F213. https://doi.org/10.1149/2.0531904jes (2019).
32. Shironita, S., Karasuda, K., Sato, K. & Umeda, M. Methanol generation by CO_2 reduction at a Pt-Ru/C electrocatalyst using a membrane electrode assembly. *J. Power Sources* **240**, 404–410. https://doi.org/10.1016/j.jpowsour.2013.04.034 (2013).
33. Bard, A. J., Parsons, R. & Jordan, J. *Standard potentials in aqueous solution* (Marcel Dekker Inc, 1985).
34. Sebastián, D. *et al.* CO_2 reduction to alcohols in a polymer electrolyte membrane co-electrolysis cell operating at low potentials. *Electrochim. Acta* **241**, 28–40. https://doi.org/10.1016/j.electacta.2017.04.119 (2017).
35. Seger, B., Vinodgopal, K. & Kamat, P. V. Proton activity in Nafion films: Probing exchangeable protons with methylene blue. *Langmuir* **23**, 5471–5476. https://doi.org/10.1021/la0636816 (2007).
36. Umeda, M., Sayama, K., Maruta, T. & Inoue, M. Proton activity of Nafion 117 membrane measured from potential difference of hydrogen electrodes. *Ionics* **19**, 623–627. https://doi.org/10.1007/s11581-012-0791-z (2013).
37. Brightman, E. & Pasquier, D. Measurement and adjustment of proton activity in solid polymer electrolytes. *Electrochem. Commun.* **82**, 145–149. https://doi.org/10.1016/j.elecom.2017.08.005 (2017).
38. Zhang, W. *et al.* Progress and perspective of electrocatalytic CO_2 reduction for renewable carbonaceous fuels and chemicals. *Adv. Sci.* **5**, 1700275. https://doi.org/10.1002/advs.201700275 (2018).
39. Wang, W., Wang, S., Ma, X. & Gong, J. Recent advances in catalytic hydrogenation of carbon dioxide. *Chem. Soc. Rev.* **40**, 3703–3727. https://doi.org/10.1039/C1CS15008A (2011).
40. Lu, J. et al. Highly efficient electrochemical reforming of CH_4/CO_2 in a solid oxide electrolyser. *Sci. Adv.* **4**, eaar5100. https://doi.org/10.1126/sciadv.aar5100 (2018).
41. Banerjee, A., Dick, G. R., Yoshino, T. & Kanan, M. W. Carbon dioxide utilization via carbonate-promoted C-H carboxylation. *Nature* **531**, 215–219. https://doi.org/10.1038/nature17185 (2016).
42. Trasatti, S. & Petrii, O. A. Real surface area Measurements in electrochemistry. *J. Electroanal. Chem.* **327**, 353–376. https://doi.org/10.1016/0022-0728(92)80162-W (1992).
43. Wang, H. *et al.* Role of Ru oxidation degree for catalytic activity in bimetallic Pt/Ru nanoparticles. *J. Phys. Chem. C* **120**, 6569–6576. https://doi.org/10.1021/acs.jpcc.5b12267 (2016).

Acknowledgements

This work was supported by JSPS KAKENHI Grant Number JP20H00282.

Author contributions

M.U. conceived the idea and supervised the entire project. M.U. and S.M. designed the experiments. Y.N. and Y.Y. performed all experiments. All authors analyzed the experimental data. S.M. wrote the paper.

Competing interests

The authors declare no competing interests.

Additional information

Supplementary Information The online version contains supplementary material available at https://doi.org/10.1038/s41598-021-87841-4.

Correspondence and requests for materials should be addressed to M.U.

Reprints and permissions information is available at www.nature.com/reprints.

Publisher's note Springer Nature remains neutral with regard to jurisdictional claims in published maps and institutional affiliations.